Development of a Direct-Drive Axial Flux Motor for Humanoids

Tomas Slimak[1], Sebastian Sterr[1] and Daniel Rixen[1]

***Abstract*— The dynamic and efficient nature of human locomotion is ever elusive to roboticists, despite the impressive progress of humanoids worldwide over the past years. Two of the driving factors of the exponential growth have been reduced costs of specialty hardware and improved modelling and control approaches. While these factors have facilitated a proliferation of impressive humanoids, there is a plateau of performance which will be reached with the current hardware solutions. To take the next step towards bio-mimetic gaits and dynamic motion, new transparent actuation concepts will be required. To this end, a direct-drive Axial-Flux Permanent-Magnet (AFPM) actuator was developed for future use in the hip joint of the humanoid robot *LOLA* at the Chair of Applied Mechanics. Insights from the design, construction, and testing of a prototype helped assess the feasibility of this actuation concept for humanoid robot locomotion. The approach employs a procedural design and analysis method, enabling the optimization and feasible construction of the actuator and its components. A critical aspect of this procedure is the use of a torque estimation equation for the analytical electromagnetic modeling of the motor. Using this sizing equation and considering various performance aspects and manufacturing constraints, a three-phase AC YASA AFPM actuator prototype with a predicted peak torque of 284 Nm at an RMS phase current of 14 A was developed (Fig. 1). Testing of the manufactured prototype resulted in a performance not matching the predictions, however this can be attributed to avoidable mechanical design deficiencies. Further studies were conducted to address the thermal and structural shortcomings. With a groundwork laid through the prototype in this work a next generation actuator can be developed for use in the humanoid robot *LOLA*.**

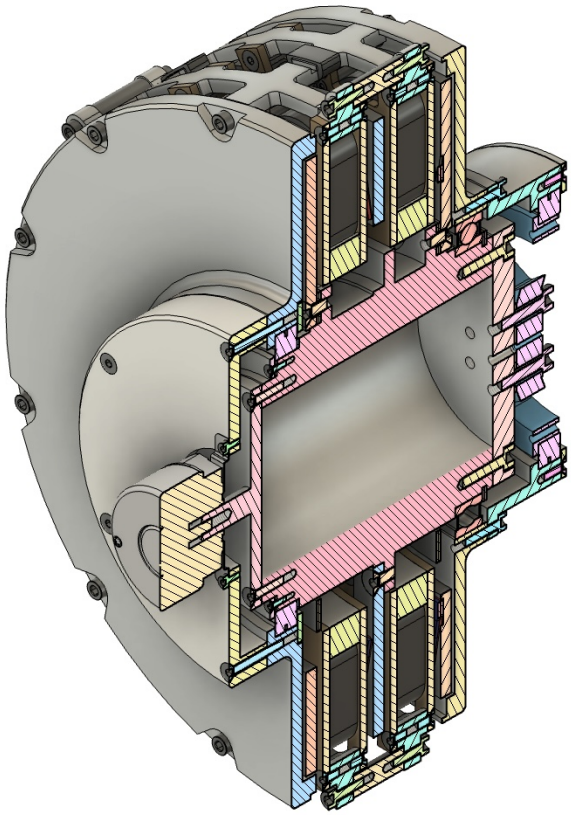

Fig. 1. Cross-sectional CAD view of the entire actuator. In this depiction the ends of the hollow axle are sealed off by the encoder and custom torque sensor [26], however both can be removed, or replaced by hollow counterparts.

I. INTRODUCTION

A. Motivation

Research in the field of biomechanics has been able to show that bipedal locomotion is largely facilitated through passive dynamics [3]. The natural design of human leg-kinematics, mass-distribution and joint stiffnesses culminates in the ability to perform steady state periodic walking with minimal active actuation. Purely through passive mechanisms such as the elastic muscle-tendon-units spanning the ankle joint or connecting the ends of the foot arch, impulsive ankle push-off can be attained [4]. The core idea of all these mechanisms is to cyclically transition from potential energy stored in springs to kinematic energy of body motion, which in turn again loads a spring. Through finely tuned timings and geometries of the foot touchdown, swapping between energy types enables human walking with minimal energy expenditure required. Actively controlled muscles still play an unquestionable role in enabling humans to perform complex non-periodic motions such as jumping, side-stepping or kicking, yet their importance during simple walking seems to be second to that of passive components. This bears the question then, why humanoid robots are actively planned and controlled through actuation at the joints with rarely any intentionally utilized elasticities [10]. One reason may be the increase in system complexity which has to be accounted for when a very specific goal or trajectory has to be reached. To maintain a high controllable bandwidth some form of model-based control has to account for the passive flexibilities and compensate their effect, often at the cost of even higher actuation effort [15]. However the advent of high-performance computing and

*This work was not directly supported by any organization, however some companies provided discounts or free samples to the university for various materials and components of the motor.

[1] Tomas Slimak, Sebastian Sterr and Daniel Rixen are with the Chair of Applied Mechanics, Technical University of Munich, 85748 Garching, Germany. If you have any questions please feel free to contact us using tomas.slimak@tum.de, we are happy to cooperate.

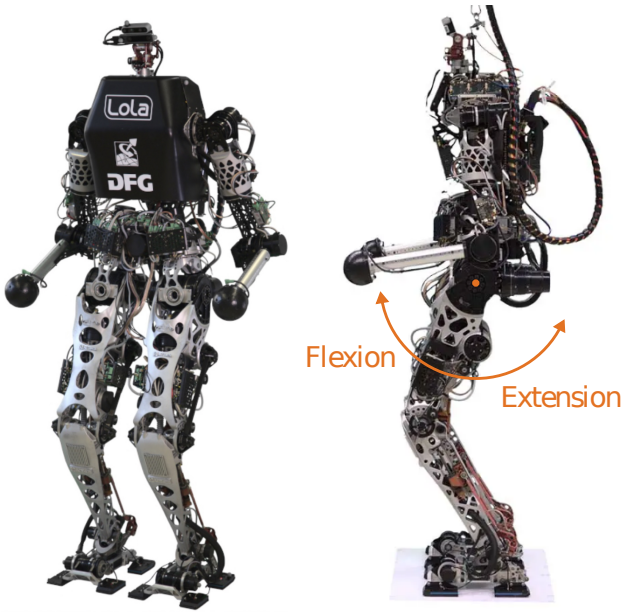

Fig. 2. The humanoid robot *LOLA*, developed at the Chair of Applied Mechanics [16]. The right image shows the robot without the upper-body cover, with the motion of the hip joint of interest highlighted in orange. [21]

data-driven modelling approaches has made it feasible to generate digital twins which accurately portray real-world dynamics, enabling control of even complex non-linear systems [29]. Another key caveat holding back the adoption of passive dynamic mechanisms in humanoid robots are the joints and actuators themselves. The finely tuned theater which swaps between energy types relies highly on the conservation of energy and friction-less backdrivable joints. Unfortunately this goal is at odds with weight optimization, which prefers smaller high-speed electric motors paired with large transmission ratios. These transmissions result in such high backdrive losses that a free swinging motion of the leg isn't possible [19]. Particularly strain-wave transmissions which posses many advantages such as high ratio at a low weight and backlash, exhibit large back-drive torques. [23]

B. Axial Flux Motors

The approach of this work is to negate the effect of transmission losses, by completely avoiding them and using a direct-drive actuator. Use of direct-drive actuation comes with additional advantages such as removing a potentially flexible link with unknown dynamics from the drive-train and not having to worry about damaging the teeth of a transmission through impact loads [6]. Unfortunately direct-drive actuators which meet the strict weight, size and torque requirements of a humanoid are not readily available. One promising avenue of research is the development of high torque density axial flux motors which are characterized by their unique dominant flux direction parallel to the rotational axis of the motor, as opposed to radially [1]. This is achieved through a pancake like arrangement of alternately stacked stator disks and magnetic rotor disks [11]. Through this arrangement, large reactive surfaces present themselves which can be used to generate high torques in small volumes. The large diameter also results in large leverarms, further increasing the torque. Despite these advantages, AFPMs aren't as ubiquitous as their radial counterpart [13]. Two attributes are responsible for this, firstly the increased manufacturing complexity and secondly the awkward form-factor. Especially when applied to humanoid robotics, only very few joints are compatible with a disk-shaped motor. Fortunately two of the pivotal joints for passive gait; the sagital hip and the knee do have the space to allow use of a disk shape. UCLA's ARTEMIS and GR-1 from Fourier Intelligence both feature Radial-Flux Permanent-Magnet (RFPM) actuators with a large diameter to enable use of low transmission ratios, thereby achieving quasi-direct actuation [6, 24]. Despite their impressive performance, the planetary gears still exhibit the disadvantage of backlash, which true direct-drive avoids. The leading industries driving the development of AFPMs in the last years are the high-performance automobile branch and windmills, where the form-factor is not as crucial as the torque density and efficiency. Examples include the Ferrari 296 GTB or the Jaguar C-X75, which utilize hybrid AFPM powertrains [35]. Unfortunately due to their vastly different requirements and boundary conditions, little can be transferred from their application to robotics.

There are currently only a few publications on the use of AFPM motors in robotics. No application of AFPM motors for the locomotion of humanoid robots could be found. Seo et al. [27] proposed an AFPM machine design intended for robotic joint applications. They presented and analyzed the design both numerically and analytically, built and tested the motor, and compared it with a RFPM brushless DC motor of the same volume. Their investigations demonstrated the AFPM motor's higher torque density. However at only 0.15 Nm without gearing, it was optimized for use with a harmonic transmission, defeating it's purpose for the application studied in this work. In the work of Yang et al. [34], a dual rotor YASA type AFPM motor was proposed for use in collaborative robot joints, chosen for its suitability in miniaturization, high torque, and high efficiency. Their design process incorporated a 3D FEA and resulted in a motor with a 24-pole/18-slot combination, achieving 1.78 Nm of rated torque, superior in torque and power density compared to a similarly sized RFPM motor, yet orders of magnitude away from humanoid requirements. Yin et al. [36] proposed an AFPM motor designed for integration into a lightweight robotic arm joint. The design optimized weight and size using specified structural dimensions and electromagnetic parameters, achieving a slim, high torque, low-speed motor with a 16-pole/12-slot configuration, producing 10.9 Nm of torque in combination with a transmission at 30 rpm. Sudano et al. [30] introduced a compact Parallel Elastic Actuator incorporating a custom AFPM motor and a non-linear magnetic torsion spring, demonstrating efficient generation of oscillatory motion for bio-inspired robotic locomotion. This work confirms that use

of AFPMs can enable natural gaits. However, the specific motor developed here only has a miniature diameter of 32 mm, making it a completely different application than the goal of this work. A vague reference was made to the use of an AFPM motor as an actuator in an exoskeleton, highlighting its high power and torque density, however no details are provided [18]. Finally, two articles by Van Damme et al. [5, 6] on specific design aspects of direct-drive AFPM actuators for robotic applications stand out. These studies focused on enhancing torque density and exploring stall torque scenarios through numerical and experimental investigations, contributing valuable insights for the development of AFPM actuators in robotics and serving as the groundwork for this study.

C. Research Outline

With the bio-inspired motivation in one hand, and the research of successfully developed AFPMs for other applications in the other hand, this work aims to develop a next generation backdrivable AFPM actuator for the hip joint of the humanoid robot *LOLA* (Fig. 2). To ultimately reach this goal, this publication presents the development of a first proof-of-concept prototype. This consists firstly of determining how to optimally size the motor to meet the desired peak torque of 243 Nm and secondly how to build and test this actuation concept. Finally, solutions to unexpected hindrances must be explored. This work aims to address the following two research questions:

1) **Are AFPM motors viable for the actuation of humanoid robots?**
2) **How does one design and build an optimal AFPM motor for robotic applications?**

After this introduction to the field of AFPM motors in the context of robotic applications and their planned incorporation into *LOLA*, the design procedure developed in this work is presented. The parametric optimization approach and the imposed boundary conditions are explained on the use-case of *LOLA's* hip motor. In the following chapter, the processes of manufacturing the individual components and assembling the prototype are described. The testing methods and their results are also presented here. Subsequently, various solutions to the issues of the motor are addressed. Finally the research questions and their answers are discussed.

II. DESIGN

In order to steer the motor design, first a set of evaluation criteria is defined. The goal isn't to reach them all immediately but to consider how they can be taken into account during the design process.

- **Electromagnetic Torque Output:** Unfortunately there is no unified definition for quantifying an actuator's peak torque τ_{pt}. Most commonly the maximum torque achievable for a few seconds is used. In this study it's defined by 5 s. The continuous torque τ_{ct}, is the sustained torque generation capacity over an indefinite period of time [9]. To match the performance of the current RFPM motor, the following should be reached: $\tau_{\mathrm{pt}} > 243$ Nm and $\tau_{\mathrm{ct}} > 122$ Nm.
- **Thermal Behavior:** Based on the industry standard for high-performance electronic components for critical applications, an upper limit working temperature of $T_{\max} = 125°\mathrm{C}$ is used. [32].
- **Backdrivability:** Actuators are already considered quasi-direct-drives with a gear ratio of 10:1 [33]. However since zero backlash is another goal, direct-drive ($N = 1$) is used here. Future iterations may include a four-bar linkage to actuate the knee joint from a motor in the hip.
- **Size and Weight:** The current actuator mass is 3.01 kg,

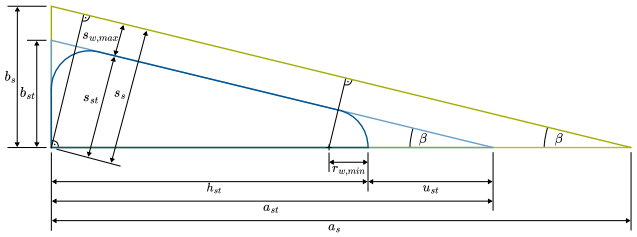

Fig. 3. The geometric relationships within the stator used to determine the dimensions of the windings and cores. Half of a core is outlined in dark blue and the boundary for the coil is outlined in green.

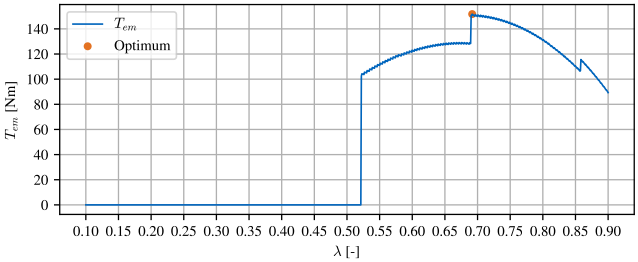

Fig. 4. The single-stator peak torque T_{em} curve, determined by the analytical sizing equation as a function of the radius ratio λ. Optimum at $\lambda = 0.692$, $T_{em} = 151.77$ Nm and magnet width of $w_m = 20$ mm. The jumps and ripple in the progression occur as a result of the discrete changes in number of windings or size of magnet used.

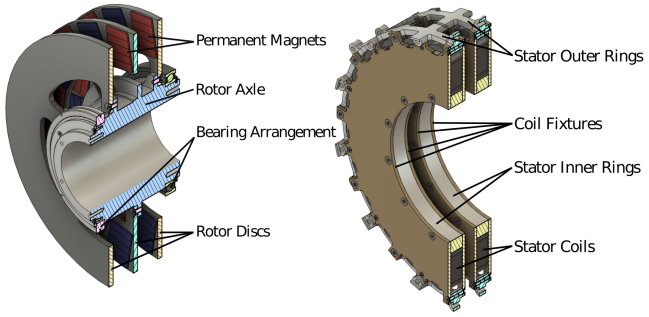

Fig. 5. Cross-sectional CAD view of the assembeled rotor on the left and stators on the right. In these depictions, the housing and sensors are not shown. The here displayed coil fixtures do not have triangular holes as seen in Fig. 8, thereby axially fixing the stator cores.

length is 183 mm and diameter is 125 mm. These can be used as reference values, however due to the different AFPM topology, it is clear that a larger diameter envelop is required. 200 mm was selected here, as it wouldn't require too much redesign of the current *LOLA* leg topoplogy.

Among AFPM actuator designs there is a plethora of possible topologies and categorizations [28]. The defining features include: number of layers [14], commutation mechanism [11], permanent magnet placement and arrangement [17], magnetic flux path configuration [20], stator construction [22] and winding configuration [12]. As searching and optimizing over this entire space of possibilities would not be feasible, the choice was made to restrict the design to the YASA-variant. It is characterized by not having a yoke (no single body connecting all the stator cores), magnets of opposing rotor disks facing each other north to south, a drum winding (winding axis = rotational axis). It was selected due to it's compact structure, lower core losses and good slot fill factor, defined as by the ratio of the conductor area to the total slot area.

In order to quickly determine the optimal geometry of the active motor components an analytical sizing approach was selected. An Ansys based FE analysis was also explored, however with unsatisfactory results and long simulation times, it wasn't used for optimization. The following analytical sizing equation, based on [31] combines all the geometric design aspects of a motor and predicts the maximal possible Torque if ideal materials were used.

$$T_{\text{em}} = \underbrace{\frac{\pi \cdot \sqrt{2}}{16}}_{i.} \cdot \underbrace{K_{w1}}_{ii.} \cdot \underbrace{A_1'}_{iii.} \cdot \underbrace{B_{g1}}_{iv.} \cdot \underbrace{\left(1-\lambda^2\right) \cdot \left(\frac{1+\lambda}{2}\right) \cdot {D_o}^3}_{v.} \tag{1}$$

i The constant YASA factor

ii The winding factor depends on the pole-slot combination of the motor. In this work, a framework is developed to determine an optimal pole-slot combination for performance optimization, considering the actuator's torque production capabilities and thermal behavior.

iii The electrical loading is based on the effective radius or diameter ratio λ and various design parameters, accounting for the pole-slot combination, conductor specifications, and stator tooth geometry based on geometrical relations.

iv The air gap flux density characterizes the air gap induction distribution. It is approximation based on geometrical relations of the stator, rotor and permanent magnets, considering various design parameters and the design variable λ.

v Motor geometry factors: These factors are dependent on λ and the machine's effective outer diameter D_o.

This sizing equation and the analytical models which determine it's factors are all defined based on the radius ratio $\lambda = R_i/R_o$ and the motor constraints, such as the number of phases $m_1 = 3$, the effective outer radius $R_o = 95$ mm and RMS phase current $I_1 = 14$ A, among others. These were selected based on limitations of the specific application, or recommendations in the literature. Building on the relationships of the sizing equation and it's factors, the geometric parameters of the stator and rotor can then be determined (Fig. 3). Fig. 4 shows the individually calculated maximal torques for various radius ratios. Upon identification of the optimal value, the ideal geometry and material of the active motor components is fixed. Based on these, the motor must next be designed. In this case, particular importance was place on the modularity and ease of future adaptions. For this reason the choice was made to not embed the stator coils in epoxy, but instead hold them from both sides with PEEK coil fixtures. Figure 8 shows the resulting design, consisting of three magnet rotor disks all attached to a single axle, and two stator disks in between. The stators are only held on the by the outer ring to the motor housing, while the inside is "freely floating" by the rotor axle. An inner ring serves the purpose of rigidifying the center to prevent axial deformations and also to absorb and redistribute thermal energy when the motor is in standstill and only a single phase is being powered, as see in Fig. 6.

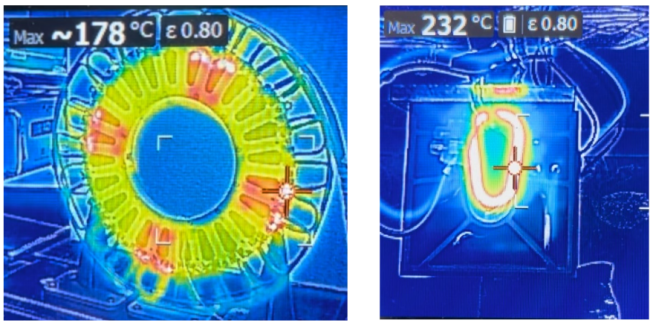

Fig. 6. Left: Phase-connection test of a single stator layer. Right: Thermal stress-test of a single stator coil.

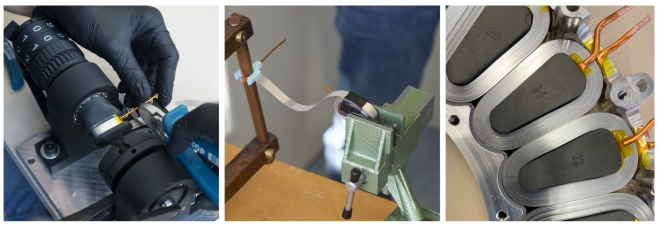

Fig. 7. Snapshots of the coil manufacturing process. Left: Trimming of the copper connector before commencing winding of the coil. Middle: The nickle-copper-aluminium stack held in a blue clip for spot welding of the connector. Right: The coils within the stator, with kapton tape in between them to protect from scratching during assembly and thermal pads at the top and bottom interfaces to the inner and outer rings.

III. MANUFACTURING AND TESTING

Sourcing and manufacturing of some of the components was particularly difficult, as they used exotic materials or required custom tools. A custom aluminium band was selected over round copper for the coils, as it has a better fill-factor, can withstand higher temperatures and use more

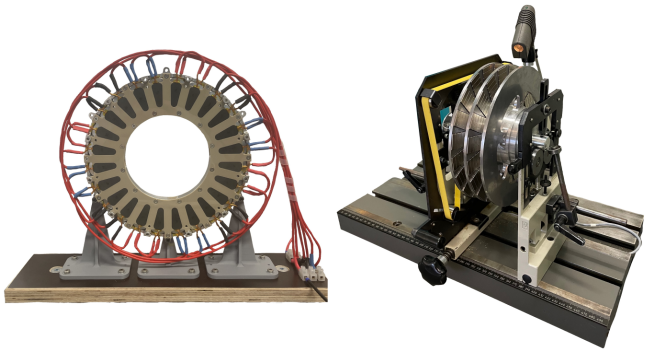

Fig. 8. Left: A single stator layer held in a test-rig. In this variation the stator cores are exposed and not held axially by the beige coil fixtures. Right: All three rotor layers connected to the axle and held within a rotor-truing machine.

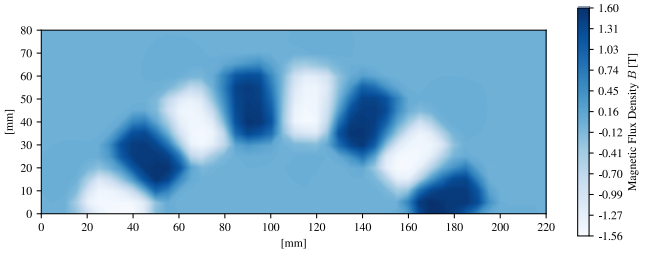

Fig. 9. The experimentally measured magnetic flux density in the axial direction 3 mm above the surface of the rotor magnets, when disassemeled from the motor. To obtain the measurements, a FM 302 Teslameter from Projekt Elektronik GmbH is mounted onto the tool flange of a GoFa CRB 15000 robot arm and automatically moved across the surface.

current. It however comes at the price of increased fragility requiring the formulation of a custom winding process. This involved the construction of a winding machine, development of a spot-welding procedure and various custom tools to carefully bring the the entire assembly together. Statistical analysis was applied to the resistances, weights, and inductivities of all the coils to filter out the outliers. Attempts were made to manufacture custom laminated sheet metal cores using electric discharge machining, however a sufficient quality could not be achieved due to de-lamination or contacting at the edges during machining. Instead soft magnetic composite cores were manufactured using a powder pressing and sintering process. Gluing of the magnets into the rotor disks required custom tools to overcome the repelling force of the magnets. Precise attention was required when bringing the stator and rotor plates together, as the powerful magnets would pull all the components together, posing a potential clamping hazard for fingers.

Tests were performed on individual sub-assemblies. Examples include the thermal tests shown in Fig. 6 where on the left one phase recieved 750 W for 5 s and where on the right single coil recieved 225 W for 10 s. Fig. 8 shows the rotor in a balancing machine. Several test runs at a balancing speed of 300 rpm measured that the rotor falls within the balancing quality grade G 2.5 according to DIN ISO 1940 and is therefore within the permissible range for high-precision applications [7]. To establish a ground truth for validation of the analytical model used for calculating the air gap flux density B_{g1} and to provide a reference for FE simulations of the actuator, a custom magnetic field measurement method for the rotor discs was developed. It uses a teslameter in combination with an automated robot arm to sample a 3D grid of point in three directions above the surface of the rotor. An example of the results can be seen in Fig. 9.

Unfortunately due to insufficient rigidity of the coil fixtures, accurate measurements of the motor torque were not possible. The powerful fields are not perfectly balanced and this results in the central free part of the stator being pulled into contact with the rotor. The surfaces press against each other with increasing force as the current grows. The friction from this contact reduces the output torque by a relatively constant factor of 3.59. Temporary solutions were attempted, such as increasing the air gap, however the contact remained, preventing an accurate evaluation of the motor performance. Before further motors can be developed this significant issue must be resolved.

Due to the contact issue, accurate thermal analysis can also not be conduced. Firstly the planned peak torque cannot be reached, secondly by being in contact, the thermal propagation within the motor is effected and lastly when operating the motor, the rubbing itself generates significant heat, falsifying any results. Tests on the individual components showed promising thermal results. Temperatures far beyond standard specifications could be maintained without implications for the electrical or structural integrity of the stators. It was apparent however that when assembled, extracting heat from the center of the motor is a problem, and could potentially be dangerous if not measured correctly.s

The outer diameter of the current prototype without cables is 220 mm and with cables 280 mm. This slightly surpassed the goal the 200 mm, however minor optimizations of the housing and custom cable routing which doesn't protrude radially could solve this issue. Axially, the new motor is only 85mm when not including the test sensors.

The current prototype weighs 7.384 kg, however no weight optimization was conducted. The mass of only the components actively responsible for torque generation is 3.958 kg, meaning that significant optimizations to the housing are possible. However the 3.01 kg of the original motor are not attainable.

IV. PROTOTYPE SHORTCOMINGS AND SOLUTIONS

Two dominant issues of the current prototype were identified; thermal management and stator stiffness. Works have begun to address both of these.

A. Thermal Management

The thermal management issue centers around the fact that the inner rings of the motor are the hottest part because they're in contact with all the coils, but have the worst access

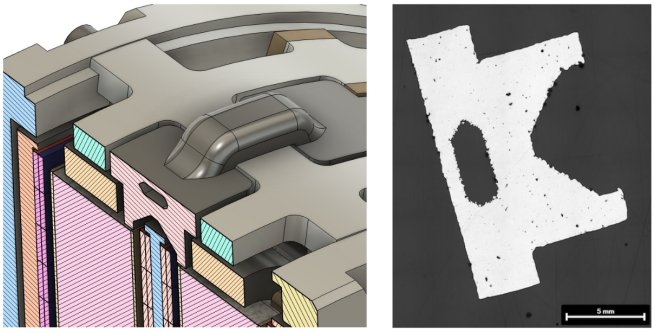

Fig. 10. Left: Cross-sectional detailed view of the outer edge of the motor with the active cooling heatsink. Right: Cross-sectional metallographical examination of porous heat-sink.

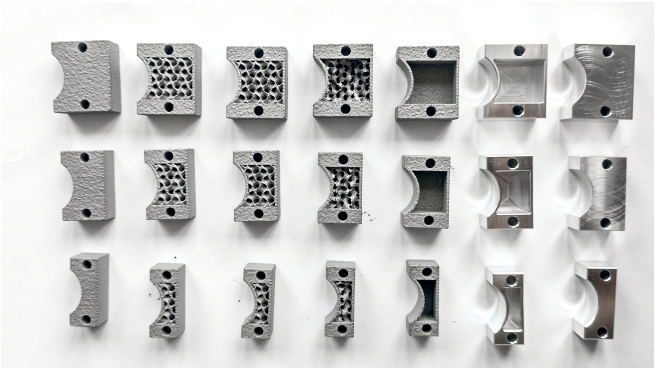

Fig. 11. Different variations of inner-ring test bodies, used to study the effect of PCMs on temperature propagation. The rows are differentiated by PCM-pocket size, while the columns are differentiated by the metal-mesh porosity or manufacturing techniques. [2]

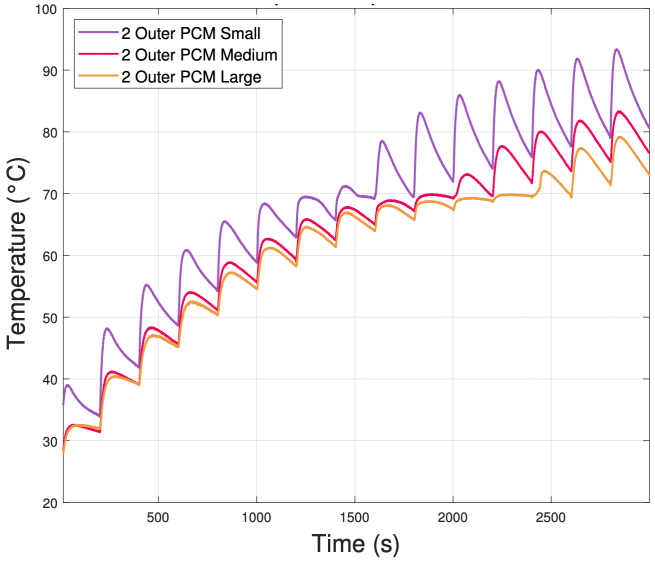

Fig. 12. A coil with 1.5% duty cycle pulses of 200 W with varying size pockets of Rubitherm 70HC PCM within a 20% metal-mesh. The plotted temperature is directly within the PCM pocket where the effect is most pronounced. It can be seen that an increase in PCM amount extends the temporary plateau at the phase-change temperature of 70°C. The constant temperature offset of the purple line is a result of experimental error, but doesn't effect the conclusion. [2]

to fresh air for dissipating their heat. To address this, two solutions are being explored; one passive and one active. The active cooling solution is a ring of metal 3D printed heatsinks which make contact the with tops of every core and and coil through teeth around the rotor, as seen in Fig. 10. Fluid is then pumped through the loop to keep the heatsinks cool. This solution does little to help at the center of the motor as contact can only be made on the outer side. The addition of a liquid cooling loop and pressurized fluid also makes the entire system more complex, dangerous and error prone. The right side of 10 shows a metallographical examination of the manufactured heatsink. The significant number of black speckles speaks to a high-porosity and increased probability of a leak during operation, which is why special care has to be taken when pumping fluilds.

The passive cooling solution has neither of these disadvantages. Pockets of PCM are embedded within the inner ring of the stator as shown in dummy inner rings in Fig. 11. The material has the ability to absorb large amounts of energy at it's transition point, without increasing in temperature, thereby keeping the coils from overheating. The disadvantage being that it also takes long for the material to cool back down. However this could still help a motor which only has to provide short pulses with long breaks in between, as could be the case for a humanoid, where very short explosive power is required to jump up or make a landing. Fig. 12 shows the results of preliminary testing, where increasing the amount of PCM material results in a prolonged plateau. One of the main disadvantages of PCM materials is their pool thermal conductivity. To counteract this metal meshes can be 3D printed into the PCM pocket. Without reducing the volume of PCM much, the thermal conductivity can be significantly improved.

B. Axial Stator Stiffness

Decreasing the bending of the stator through increase of stiffness can be done in two ways; either through increase of coil holding material, or through change of material. Both approaches carry potentially negative consequences for the motor. By increasing the amount of material, the gap between the magnets and the coils increases, reducing the output torque. Switching to a different material like metal could change the magnetic field paths or facilitate eddie-currents. Alternative carbon-fibre or glass-fibre solutions may be a possibility but their manufacturing is difficult due to the health hazards of milling fibres.

The standard solution in industrial motor manufacturing to fix stators and prevent movement is embedding them in epoxy. Given the costly and time-intensive nature of producing the coils any irreversible process has been avoided so far. The temperamental nature of resin curing, also makes this an approach with significant risk of failure.

V. CONCLUSIONS

The objective of this study was to develop a direct-drive AFPM actuator for the flexion and extension of the hip joint in the humanoid robot LOLA. The design and construction

of a prototype, along with performance tests, were aimed at evaluating the feasibility of this actuation concept for humanoid robot locomotion. Through a parametric sizing equation, an optimized electromagnetic motor model was identified. This modeling and optimization process resulted in a three-phase AC YASA AFPM actuator concept in a two-stage multi-stator-multi-rotor configuration, featuring a 20-pole/24-slot combination per stage, and an estimated peak torque of 283.60 Nm at an RMS phase current of 14 A. Building upon the optimized motor concept and considering various performance and manufacturing-specific aspects, the detailed actuator design was developed, and the prototype was constructed. This prototype could not be properly evaluated due to structural issues of the stator. Nevertheless, an automated motor design pipe-line was successfully created and tested. Thanks to it's modular nature, the resulting prototype can now be used as a test-bed for future research.

ACKNOWLEDGMENTS

The authors would like to thank the following students for their contributions to this paper: Michael Piltz for his work on developing thermal and magneto-static simulations of the motor [25], Maximilian Bakker-Müller for his study of cooling solutions for the motor [2], Maksim Eibozhenko for his testing of alternative stator holders [8].

REFERENCES

[1] Shahbaz Amin, Sahib Khan, and Syed Sabir Hussain Bukhari. "A Comprehensive Review on Axial Flux Machines and Its Applications". In: *2019 2nd International Conference on Computing, Mathematics and Engineering Technologies (iCoMET)*. 2019, pp. 1–7. DOI: 10.1109/ICOMET.2019.8673422.

[2] Maximilian Bakker-Müller. "An Exploration of Optimal Cooling Solutions for Axial Flux Motors". Chair of Applied Mechanics, Technische Universität München, Apr. 2024.

[3] Alexandra Buchmann et al. "Power to the Springs: Passive Elements are Sufficient to Drive Push-Off in Human Walking". en. In: *Robotics in Natural Settings*. Springer International Publishing, 2022. ISBN: 9783031152529783031152269. DOI: 10.1007/978-3-031-15226-9_5.

[4] Alexandra Buchmann et al. "The effect of including a mobile arch, toe joint, and joint coupling on predictive neuromuscular simulations of human walking". en. In: *Scientific Reports* 14.1 (2024). DOI: 10.1038/s41598-024-65258-z.

[5] Jordi Van Damme, Hendrik Vansompel, and Guillaume Crevecoeur. "Anodized Aluminum Foil Winding Axial Flux Machine for Direct-Drive Robotic Applications". In: *IEEE Transactions on Industrial Electronics* 70.10 (Oct. 2023), pp. 10409–10419. DOI: 10.1109/tie.2022.3220894.

[6] Jordi Van Damme, Hendrik Vansompel, and Guillaume Crevecoeur. "Stall Torque Performance Analysis of a YASA Axial Flux Permanent Magnet Synchronous Machine". In: *Machines* 11.4 (Apr. 2023), p. 487. DOI: 10.3390/machines11040487.

[7] *DIN ISO 1940 Teil 1: Anforderungen an die Auswuchtgüte starrer Rotoren - Bestimmung der zulässigen Restunwucht*. Berlin: Beuth Verlag GmbH, Dec. 1993.

[8] Max Eibozhenko. "Structural Optimization of an Axial Flux Motor". Chair of Applied Mechanics, Technische Universität München, 2024.

[9] George Ellis. *Control system design guide*. 4th ed. Butterworth-Heinemann, June 2012. ISBN: 978-0123859204.

[10] Grzegorz Ficht and Sven Behnke. "Bipedal Humanoid Hardware Design: a Technology Review". In: *Current Robotics Reports* 2.2 (Apr. 2021), pp. 201–210. DOI: 10.1007/s43154-021-00050-9.

[11] Jacek F Gieras, Rong-Jie Wang, and Maarten J Kamper. *Axial Flux Permanent Magnet Brushless Machines*. en. 2nd ed. New York, NY: Springer, Apr. 2008.

[12] Asiful Habib et al. "A fully coreless Multi-Stator Multi-Rotor (MSMR) AFPM generator with combination of conventional and Halbach magnet arrays". In: *Alexandria Engineering Journal* 59.2 (Apr. 2020), pp. 589–600. DOI: 10.1016/j.aej.2020.01.039.

[13] Asiful Habib et al. "A systematic review on current research and developments on coreless axial-flux permanent-magnet machines". In: *IET Electric Power Applications* 16.10 (June 2022), pp. 1095–1116. DOI: 10.1049/elp2.12218.

[14] Zhuo Hao et al. "A Review of Axial-Flux Permanent-Magnet Motors: Topological Structures, Design, Optimization and Control Techniques". In: *Machines* 10.12 (2022). ISSN: 2075-1702. DOI: 10.3390/machines10121178.

[15] Shayan Hoshyari et al. "Vibration-minimizing motion retargeting for robotic characters". In: *ACM Trans. Graph.* 38.4 (July 2019). ISSN: 0730-0301. DOI: 10.1145/3306346.3323034.

[16] *Humanoid Robot LOLA*. Accessed July 15, 2024.

[17] Solmaz Kahourzade et al. "A Comprehensive Review of Axial-Flux Permanent-Magnet Machines". In: *Canadian Journal of Electrical and Computer Engineering* 37.1 (2014), pp. 19–33. DOI: 10.1109/cjece.2014.2309322.

[18] *KAIST Exoskeleton Laboratory (Exo Lab) - Robot Team's Research Area - Actuator Module Design*. 2019.

[19] Navvab Kashiri et al. "An Overview on Principles for Energy Efficient Robot Locomotion". In: *Frontiers in Robotics and AI* 5 (Dec. 2018). ISSN: 2296-9144. DOI: 10.3389/frobt.2018.00129.

[20] Ju Hyung Kim, Wooyung Choi, and Bulent Sarlioglu. "Closed-form solution for winding types of axial flux permanent magnet machines". In: *2014 IEEE Energy Conversion Congress and Exposition (ECCE)*. IEEE, Sept. 2014. DOI: 10.1109/ecce.2014.6954208.

[21] *Lola - Robots: Your Guide to the World of Robotics*. Accessed July 15, 2024.

[22] Amin Mahmoudi, Nasrudin Abd Rahim, and Wooi Hew. "Axial-flux permanent-magnet machine modeling, design, simulation and analysis". In: *Scientific Research and Essays* 6 (July 2011), pp. 2525–2549.

[23] Tobias Nef and Peter Lum. "Improving backdrivability in geared rehabilitation robots". In: *Medical & Biological Engineering & Computing* 47.4 (Jan. 2009), pp. 441–447. ISSN: 1741-0444. DOI: 10.1007/s11517-009-0437-0.

[24] Frederik Ostyn, Bram Vanderborght, and Guillaume Crevecoeur. "Design and Control of a Quasi-Direct Drive Robotic Gripper for Collision Tolerant Picking At High Speed". In: *IEEE Robotics and Automation Letters* 7.3 (July 2022), pp. 7692–7699. ISSN: 2377-3774. DOI: 10.1109/lra.2022.3184777.

[25] Michael Piltz. "Electromagnetic Simulation for the Optimal Design of an Axial Flux Motor". Chair of Applied Mechanics, Technische Universität München, Mar. 2023.

[26] Gawan Russek. "Development, Production and Calibration of a Torque Sensor for a Robot Joint". Chair of Applied Mechanics, Technische Universität München, Oct. 2022.

[27] Jung-Moo Seo et al. "Design of axial flux permanent magnet brushless DC motor for robot joint module". In: *The 2010 International Power Electronics Conference - ECCE ASIA -*. IEEE, June 2010. DOI: 10.1109/ipec.2010.5544557.

[28] Lingyun Shao et al. "Design and Construction of Axial-Flux Permanent Magnet Motors for Electric Propulsion Applications—A Review". In: *IEEE Access* 9 (2021), pp. 158998–159017. DOI: 10.1109/access.2021.3131000.

[29] Tomas Slimak et al. "Overview of Design Considerations for Data-Driven Time-Stepping Schemes Applied to Nonlinear Mechanical Systems". In: *Journal of Computational and Nonlinear Dynamics* 19.7 (June 2024), p. 071012. ISSN: 1555-1415. DOI: 10.1115/1.4065728.

[30] Angelo Sudano et al. "A resonant parallel elastic actuator for biorobotic applications". In: *2014 IEEE/RSJ International Conference on Intelligent Robots and Systems*. IEEE, Sept. 2014. DOI: 10.1109/iros.2014.6942948.

[31] Rodrigo B. Tavares et al. "Torque Assessment of Multiphase AFPM Machines With Experimental Validation for YASA Topology". In: *IEEE Transactions on Energy Conversion* 38.1 (Mar. 2023), pp. 111–121. ISSN: 1558-0059. DOI: 10.1109/tec.2022.3187644.

[32] *TWI global - Technical Knowledge - FAQs - At what temperature do conventional electronics packages fail?* 2024.

[33] Jürgen Wagenbach. *Gears: Self-locking or back-drivability – Maxon Support*. May 2023.

[34] Seo-Hee Yang et al. "A Study on Optimal Design Process of Dual Rotor Axial-Flux Permanent Magnet Synchronous Motors". In: *Machines* 11.4 (Apr. 2023), p. 445. DOI: 10.3390/machines11040445.

[35] *YASA Engineering Revolution - Applications*. Accessed March 20, 2024.

[36] Haibin Yin, Yanming Yu, and Junfeng Li. "Optimization design of a motor embedded in a lightweight robotic joint". In: *2017 12th IEEE Conference on Industrial Electronics and Applications (ICIEA)*. IEEE, June 2017. DOI: 10.1109/iciea.2017.8283100.